Hydrol. Earth Syst. Sci. Discuss., 11, 7689–7732, 2014
www.hydrol-earth-syst-sci-discuss.net/11/7689/2014/
doi:10.5194/hessd-11-7689-2014

Hydrology and Earth System Sciences
Open Access
Discussions

Agro-hydrology and multi temporal high resolution remote sensing: toward an explicit spatial processes calibration

S. Ferrant[1,2], S. Gascoin[1,3], A. Veloso[1,3], J. Salmon-Monviola[4,5], M. Claverie[6,7], V. Rivalland[1,3], G. Dedieu[1,2], V. Demarez[1], E. Ceschia[1], J.-L. Probst[8,9], P. Durand[4,5], and V. Bustillo[1]

[1]Université de Toulouse, UPS, Centre d'Etude Spatiale de la BIOsphère (CESBIO), 18 av. Edouard Belin, bpi 2801, 31401 Toulouse, cedex 9, France
[2]Centre National d'Etudes Spatiales (CNES), CESBIO, Toulouse, France
[3]CNRS-CESBIO, Toulouse France
[4]INRA – UMR1069 Sol Agro et hydrosystème Spatialisation (SAS), 35000 Rennes, France
[5]Agrocampus Ouest, UMR1069, SAS, 35000 Rennes, France
[6]Department of Geographical Sciences, University of Maryland, College Park, MD 20742, USA
[7]NASA-Goddard Space Flight Center, Greenbelt, MD 20771, US
[8]Université de Toulouse, UPS, INPT, Laboratoire d'Ecologie Fonctionnelle et Environnement (EcoLab), ENSAT, Avenue de l'Agrobiopole, BP 32607 Auzeville-Tolosane, 31326 Castanet-Tolosan Cedex, France

[9]CNRS, Ecolab, ENSAT, Avenue de l'Agrobiopole, Castanet, France

Received: 29 May 2014 – Accepted: 24 June 2014 – Published: 10 July 2014

Correspondence to: S. Ferrant (sylvain.ferrant@cesbio.cnes.fr)

Published by Copernicus Publications on behalf of the European Geosciences Union.

Abstract

The recent and forthcoming availability of high resolution satellite image series offers new opportunities in agro-hydrological research and modeling. We investigated the perspective offered by improving the crop growth dynamic simulation using the distributed agro-hydrological model, Topography based Nitrogen transfer and Transformation (TNT2), using LAI map series derived from 105 Formosat-2 (F2) images during the period 2006–2010. The TNT2 model (Beaujouan et al., 2002), calibrated with discharge and in-stream nitrate fluxes for the period 1985-2001, was tested on the 2006–2010 dataset (climate, land use, agricultural practices, discharge and nitrate fluxes at the outlet). A priori agricultural practices obtained from an extensive field survey such as seeding date, crop cultivar, and fertilizer amount were used as input variables. Continuous values of LAI as a function of cumulative daily temperature were obtained at the crop field level by fitting a double logistic equation against discrete satellite-derived LAI. Model predictions of LAI dynamics with a priori input parameters showed an temporal shift with observed LAI profiles irregularly distributed in space (between field crops) and time (between years). By re-setting seeding date at the crop field level, we proposed an optimization method to minimize efficiently this temporal shift and better fit the crop growth against the spatial observations as well as crop production. This optimization of simulated LAI has a negligible impact on water budget at the catchment scale (1 mm yr^{-1} in average) but a noticeable impact on in-stream nitrogen fluxes (around 12 %) which is of interest considering nitrate stream contamination issues and TNT2 model objectives. This study demonstrates the contribution of forthcoming high spatial and temporal resolution products of Sentinel-2 satellite mission in improving agro-hydrological modeling by constraining the spatial representation of crop productivity.

HESSD

11, 7689–7732, 2014

Agro-hydrology and multi temporal high resolution remote sensing

S. Ferrant et al.

1 Introduction

Agro-hydrological modeling has been early developed and used to study the qualitative and quantitative impact of agriculture on water resources in cropped land areas (Arnold et al., 1993, 1998; Breuer et al., 2008; Engel et al., 1993; Galloway et al., 2003; Leonard et al., 1987; Refsgaard et al., 1999; Whitehead et al., 1998). Hydrology and crop models have been coupled to take into account influences of both hydrological settings and of agricultural practices on the water and nutrient cycle at the agricultural catchment scale: CWSS (Reiche, 1994), DAISY/MIKE-SHE (Refsgaard et al., 1999), NMS (Lunn et al., 1996), SWAT (Arnold et al., 1998), INCA (Whitehead et al., 1998), SHETRAN (Birkinshaw and Ewen, 2000), TNT2 (Beaujouan et al., 2002), DNMT (Liu et al., 2005), STICS-MODCOU-NEWSAM (Ledoux et al., 2007). Since, these approaches have been widely used; hundred of publications, among which SWAT model is probably the most widely used, report their use to study the impact of (1) agriculture in term of stream water quality, e.g. nitrate contamination (Durand, 2004; Ferrant et al., 2011), (2) agricultural land use scenarios to assess agricultural policy efficiency in term of achievement of environmental objectives (Volk et al., 2009), (3) best agricultural practices in terms of stream water quality (Ferrant et al., 2013; Laurent et al., 2007), (4) climate change impacts on surface water (Franczyk and Chang, 2009) or groundwater and irrigation withdrawal (Ferrant et al., 2014), (5) hydrologic impoundments and wetland on water resources (Bosch, 2008; Perrin et al., 2012).

1.1 Spatially explicit modeling

Most of these applications require spatially distributed models, where information of soil-crop location within slopes as well as hydrological settings (topography, groundwater storage, reservoir location or irrigation pumping) are included to provide spatially explicit information on water uses (Ferrant et al., 2014; Perrin et al., 2012) and nutrients transfer and transformation within the catchment (Arnold et al., 1998; Beaujouan et al., 2002; Ferrant et al., 2011). These modeling approaches allow studying the interactions

HESSD
11, 7689–7732, 2014

between upland and bottomland fields, groundwater table fluctuation and nitrogen cycle in the soil-plant system. They are especially relevant to localize the sources and sinks of nitrogen within landscapes: areas prone to nitrogen leaching vs. areas prone to nitrogen retention which are dynamically changing depending on cropping patterns and hydrological conditions. The spatial resolution of the simulated processes is linked to the resolution of the available input data (land use, soil, aquifer and topography maps). High resolution data may eventually be required to accurately assess the impact of agricultural practices on water resources. Perrin et al. (2012) used the SWAT model to simulate the groundwater storage under high agricultural pumping rate in South India. They used high resolution optical satellite images (between 5 to 10 m) to derive the spatial groundwater extraction from the irrigated area extent. This high spatial resolution of pumping rates coupled with hydro-geological settings maps are used within SWAT to identify areas prone to exhaust groundwater resources under nowadays uses for present and future climate (Ferrant et al., 2014).

1.2 Limitations of current distributed modeling

In complex distributed agro-hydrological models simulating numerous processes, having numerous parameters to spatially represent the temporal dynamic of water and nutrient cycle and crop growth, conventional stream flow calibration may lead to equifinality problems, e.g. more than one parameter leading to similar results (Beven, 2001) or compensation between processes leading to similar stream water fluxes (Ferrant et al., 2011). Uncertainties raised by these modeling approaches at the watershed level are mainly related to (1) the lack of agronomical observations in all soil-climatic situations encountered within the catchment, i.e. crop biomass production and the partition between exportation by harvest or incorporation within soil organic matter by straws burial, (2) the lack of spatial a priori knowledge, such as soil organic matter transformations, saturated conditions within slopes and their feedback on crop productivity. Indeed, the calibration process is limited to optimizing integrative variables at the watershed scale: discharge and nutrient fluxes at the outlet, sometimes average crop yield

(Ferrant, 2009; Ferrant et al., 2011; Moreau, 2012), or more rarely aquifer recharge (Perrin et al., 2012). Another important aspect of the uncertainty raised by these modeling approaches is that agricultural operations are not known perfectly. Hutchings (2012) have demonstrated the importance of the timing of field operations on complex dynamic carbon and nitrogen models. For instance, winter crops growth in Europe are highly sensitive to the time of the first fertilization as well as the seeding date.

1.3 Expectations from remote-sensing technology

This picture suggests that spatially explicit process modeling requires a better spatial and temporal calibration to strengthen the spatial representation of C, N and water cycles at the catchment scale. Remote sensing (RS) derived products are promising tools to better constrain and spatially calibrate agro-hydrological models. Land cover, and sometimes landuse (temporal cropping patterns) derived from RS are generally introduced as input variables. But RS products have been only parsimoniously used in calibration processes. Wagner et al. (2009) have reviewed RS techniques used in hydrological models to force RS derived variables as: soil moisture, evaporation, snow cover, vegetation structure, hydrodynamics roughness. Much of these studies used low spatial resolution imagery like Moderate Resolution Imaging Spectro radiometer (MODIS), scatterometer data, microwave and radiometer data (Brocca et al., 2009, 2012; Laguardia and Niemeyer, 2008; Liu et al., 2009). Nagler (2011) reviewed the recent advances in our knowledge of evaporation on an environmental scale over the past decades by using remote sensing. For instance, Chen et al. (2005) have calibrated a TopModel (Beven, 1997) derived hydrological model in a small forested catchment using RS Leaf Area Index (LAI, surface of vegetation cover in m^2 for a ground surface in m^2) and AET obtained from an Eddy covariance tower measurement, in order to assess the impact of topography on AET.

More specifically, some studies have demonstrated the potential interest of using RS derived AET and LAI in agro-hydrological models to quantify water balance components in irrigated areas (Taghvaeian and Neale, 2011). AET derived from satellite products have been used to spatially calibrate SWAT during short time study period (Cheema et al., 2014; Immerzeel and Droogers, 2008; Immerzeel et al., 2008). Cheema et al. (2014) combined global extraterrestrial radiation with atmospheric transmissivity derived from 1 km pixel resolution MODIS to compute a local net radiation at the Indus catchment scale. This latter is used to compute the evapotranspiration using the Penman–Monteith algorithm. The SWAT model is then calibrated on this spatial representation of evapotranspiration fluxes for all hydrological response units. This spatial calibration method presented in this recent study is still limited by the resolution gap between evapotranspiration products at a moderate resolution and the patchy pattern of irrigated area that need to be described at a high spatial resolution. Another promising example of RS products used in crop model calibration is reported by Jégo et al. (2012). These autors used Leaf Area Index (LAI) retrieved from RS data to re-set selected input parameters of the functional crop model STICS (Brisson, 1998). They demonstrated that the predicted yield and biomass were improved, especially in the case of water-stress conditions. Considering the distributed agro-hydrological model TNT2, which is based on STICS spatially coupled with a hydrological model TNT derived from TopModel hypothesis, a calibration of crop input parameters could be performed by matching simulated and observed LAI at the crop field level. The question is whether the spatial calibration of the LAI dynamics using LAI map series derived from high resolution RS data may have an impact on water and nutrient fluxes as compared with a standard calibration using discharge. Indeed, this calibration method would require high spatial resolution images with 4/5 days of revisiting period which will be provided by two satellite missions: Venμs (Dedieu et al., 2006) and Sentinel-2. Sentinel-2 type time series have been previously used to constrain crop models such as SAFY (Duchemin et al., 2008) for monitoring crop growth and estimating crop production (Claverie, 2012). SAFY is a semi-empirical model, based on the light-use efficiency theory, with limited number of input parameters and formalisms. It describes the main biophysical processes, driven by climatic data and using empirical parameterizations. Therefore this simplified model is efficient for operational crop growth diagnosis/studies over large areas, but at this stage it cannot be used to project different climatic and environmental scenarios. Contrary to these models, agro-hydrological models (like TNT2 or SWAT for instance) are designed to take into account climate change impacts on crop growth and hydrological variables for prospective research. Provided that large amount of input data are available within areas of interest, physical knowledge-based base agro-hydrological models can benefit from the use of HTSR RS products to better simulate the spatial distribution of complex and detailed processes.

1.4 Objectives

The aim of the present study is therefore to explore the gain of using Leaf Area Index maps series derived from high resolution RS products on the spatial representation of water and nutrient fluxes of an agro-hydrological model. This study focuses on an experimental catchment where intensive monitoring of stream water discharge and nitrate concentration has been used to calibrate a distributed agro-hydrological model (TNT2) for the period 1985–2001 (Ferrant et al., 2011) by taking into account climatic variables, crop rotation and agricultural practices. From this starting point, the calibrated model TNT2 was run on a new agricultural and climatic data set for the 2006–2010 period. A set of 105 LAI maps derived from Formosat-2 images (8 m resolution) has been used to optimize LAI temporal growth by iteratively re-setting seeding date at the crop field level. Indeed, this input is often not reported; missing values are estimated using existing recorded seeding date. Re-setting seeding date is th way to shift crop growth in time. We explore the impact of this spatial optimization using LAI maps derived from optical RS in term of water and nitrogen budget at the catchment level.

2 Material and methods

2.1 Study site presentation

The Montoussé catchment at Auradé (Gers, France) is an experimental research site monitored since 1983 to investigate the impact of fertilizers on stream water quality. Nitrate measurements in the stream began in 1985 by the fertilizer manufacturer GPN-TOTAL to assess the impact of agricultural practices and landscape management on nitrate concentrations in stream water. The catchment was selected for intensive survey because of its fast hydrological response in an intensive agricultural context. Crop rotation system consists mainly in a sunflower and winter wheat rotation, fertilized only with mineral fertilizers. The Fig. 1 illustrates the agronomical and hydrological situation of the study site. As a tributary channel of the Save River, itself a left tributary of the Garonne River, the catchment area is representative of a wider agricultural area embedded within the Gascogne region in south-west of France where similar agricultural and geomorphologic settings are found (Ferrant, 2009). This small catchment (3.35 km^2) is hilly and 88.5 % of the surface is cultivated. The substratum consists of impervious Miocene molassic deposits; a shallow aquifer lies on this clayey layer which is highly heterogeneous by composition. Groundwater that is sparsely distributed within sand lenses located at mid-slope and within deep alluvial soils bordering the stream network are the main providers of the river discharge during low flow periods.

A soil mapping of the catchment was carried out in 2006 by Sol-Conseil and EcoLab presented in Ferrant et al. (2011). Twelve soil types were identified along a topography sequence, from deepest soil in bottomland (around 2 m) to shallowest soils from middle slope to top of slope (in between 1 m to 30 cm). These agricultural soils exhibit low organic carbon (1.1 to 2 % in the first cm to 0.4 % in deep horizon) and high clay contents (25 to 40 % in the first cm to 50 % in deep horizon). Each soil map unit represents an area where a dominant soil type is found. Even if the delineation is based on 200 auger drilling in 325 ha, this map remains a reliable proxy of the fine variability of soil characteristics observed in the field.

HESSD
11, 7689–7732, 2014

The climate is under the influence of both the Oceanic and the Mediterranean climate. Mean annual rainfall recorded in the study site for the 1985–2001 period was 656 mm with a minimum of 399 and a maximum of 844 mm yr^{-1}. The maximum daily rainfall observed during this period was 90 mm; these intense rainfall events are observed during spring and autumn and generate large runoff events of less than one day. Average daily temperatures were 14.5 °C, varying from 0–1 °C in winter and 29–30 °C in summer, leading to an average potential evapotranspiration (PET) of 1020 mm yr^{-1}. The period 2006–2010 is marked by similar annual precipitations: mean was 664 mm yr^{-1}, varying from 628 to 737 mm yr^{-1} but hot spring and summer have led to a higher PET (1039 mm yr^{-1}). The annual discharge at the outlet is highly variable (from 6 to 33 % of the rainfall in the 1985–2001 period) and represents 4 to 15 % of the rainfall during the 2006–2010 study period. This period is drier in terms of hydrological conditions than the historical period used to calibrate the TNT2 model.

A hydro-chemical data base containing daily discharges and high frequency nitrate concentration measurements have been filled and maintained by the AZF company from 1985 to 2001 and has been used to study the nitrate contamination of the stream water at the catchment scale (Ferrant et al., 2013, 2011). From this nitrate oriented monitoring protocol, many more recent systematic observations and measurements were implemented to improve the understanding of the main processes that drive water, nutrient and carbon fluxes in the agro-ecosystem and that are subjected to be impacted by global changes.

2.2 Study period (2005–2010) and ground data

2.2.1 Hydro-chemistry

Stream water nitrate concentrations and discharge were continuously monitored at the outlet of the catchment for the 2006–2012 period (measurement protocol and data are fully described in Ferrant et al. (2012). From continuous recorded signal, nitrate and water fluxes at the outlet of the catchment are aggregated at a daily time step to match the modeling time step.

2.2.2 Agricultural practices survey

Annual enquiries about agricultural land cover and practices are collected among volunteer farmers within the framework of the farmer association "association des agriculteurs d'Auradé". Seeding dates, tillage operations, fertilizer application and crop harvest dates, amount of fertilizer applied, constitutes the basic agricultural practices filled by farmers for each crop field. This participative survey never reaches 100 % of participation; many crop field operations remain unknown. For a given year, missing seeding dates, fertilization amount and dates are deduced from existing recorded practices. Contrary to that, the crop rotation is known for the entire area during the study period. We crossed the land cover information contained within the "Registre Parcellaire Graphique" (RPG) data base with crop cover mapping using supervised classification of Formosat-2 and SPOT images. The RPG is based on annual farmer declaration of the land cover for crop field blocks, statement which is mandatory by the European Common Agricultural Policy (CAP). However, both sources of information gives the crop type (wheat, sunflower, rapeseed, barley), but no indication of the cultivar used. The main uncertainty of this agricultural data base is linked to the seeding and fertilization dates, as well as fertilization amount. We will refer to this agricultural practices data as "a-priori" as they are constructed using non exhaustive enquiries and used for a first run of the TNT2 model.

2.2.3 Atmospheric turbulent fluxes

Atmospheric flux instruments were set in March 2005, located in an experimental crop plot at 800 m of the eastern part of the catchment (Fig. 1). Turbulent fluxes of CO_2, water vapor (actual Evapotranspiration and latent heat), sensible heat and momentum are continuously measured by the Eddy Covariance method (Baldocchi et al., 1988). Field vegetation measurements were also performed to study the carbon balance and crops water use efficiencies of the cropping pattern (Béziat et al., 2009; Tallec et al., 2013). The daily actual evapotranspiration (AET) measurements derived from this equipment will be compared with the AET simulated by the model for a similar crop location located inside the catchment.

2.2.4 Vegetation dynamics measurements

Destructive measurements of vegetation dynamics are carried out on the experimental plot during each crop season of the study period. They consisted in estimating Leaf Area Index and Green Area Index (LAI and GAI) completed by aerial biomass measurements at main development stages (Béziat et al., 2009). 10 and 30 plants were collected on two diagonals of the fields for respectively wheat and sunflower. Sampling frequency was adapted to the vegetation development, from the month during slow vegetation development period to two weeks during fast vegetation development period. LAI and GAI were measured by means of a LiCor planimeter (LI3100, LiCor, NE, USA). Between each destructive measurement date, several randomly spatially distributed hemispherical photographs were taken to catch the leaf development dynamic. The camera used for these measurements, a Nikon CoolPix 8400 equipped with a FC-E8 fisheye lens, was put on the top of a pole to keep the viewing direction (looking downward) and canopy to sensor distance constant (1.5 m) throughout the growing season. The hemispherical photographs were processed using CAN-EYE V5 (http://www4.paca.inra.fr/can-eye), which provides an effective GAI (Baret et al., 2010; Demarez et al., 2008) for the whole picture. These data were used to assess the model accuracy to reproduce the biomass production and LAI dynamics of crops. A field crop comparable to the experimental plot in term of situation and cropping pattern was selected within the catchment; it is called crop field (8) hereafter (Fig. 1).

HESSD
11, 7689–7732, 2014

2.3 Leaf Area Index maps derived from Formosat-2 data

We used optical remote sensing data from Formosat-2 (F2; Chern et al., 2006) to estimate the LAI for each pixel of the ground coverage area (see in Fig. 1). F2 is a high spatial (8 m) and temporal (daily revisit time) resolution satellite with four spectral bands (488, 555, 650 and 830 nm) and a swath of 24 km. For a given site, F2 data may be acquired every day under a constant viewing angle. This characteristic was used to perform accurate atmospheric corrections by estimating the aerosol optical thickness using a multi-temporal method (Hagolle et al., 2008). All F2 images were first pre-processed for geometric, radiometric and atmospheric corrections as well as cloud and cloud-shadow filtering (Hagolle et al., 2010).

105 LAI maps at 8 m resolution encompassing the whole catchment (ground coverage shown in Fig. 1) were derived from 105 Formosat-2 images in 5 years (2006–2010) using the BV-NNET tool (Biophysical Variable Neural NETwork; Baret et al., 2007). BV-NNET is based on the inversion of a radiative transfer model (PROSAIL; Jacquemoud et al., 2009) using artificial neural networks. The LAI retrieval method is fully described in Claverie (2012) and Claverie et al. (2013). A main advantage of this method is that it does not require any prior calibration with in-situ measurements.

The land cover within the experimental catchment was derived from field survey and F2 images supervised classification ref? at the crop field level. These maps series are used to explore the spatial and temporal heterogeneity in terms of crop growth at the pixel and crop field level. Daily values of LAI as a function of cumulative daily temperature were obtained by fitting a double logistic equation against discrete satellite-derived LAI (see equation in Fig. 2) at both crop field and pixel levels. The results at the pixel level are used to discuss the spatial variability of the crop development observed within slopes and fields, whereas the results at the crop field level are used in the optimization procedure described in the Fig. 4.

HESSD
11, 7689–7732, 2014

2.4 TNT2 agro-hydrological model

TNT2 is a process-based and spatially distributed model developed to study N fluxes and water cycle in small agricultural catchments (< 50 km^2). The model combines the crop model STICS (version 4) and the hydrological model TNT (Beaujouan et al., 2002).

The TNT2 model has been successfully calibrated on the Auradé experimental catchment for the water and nitrogen fluxes at the outlet for a long period of time (1985–2001; Ferrant et al., 2011). TNT2 inputs and parameters include 4 types of spatial information: (i) a landscape pattern delineating the agricultural plots, roads, hydrological network and landscape features (wetlands, hedgerows, etc.), (ii) a soil map, (iii) a climate map of climate gradients within the catchment, (iv) agricultural practices associated to a crop sequence for each agricultural plot during the simulation period.

The TNT2 agronomical module is based on STICS modeling approach (Brisson, 1998): it is a generic model that simulates crop growth at the plot scale with the input of agricultural practices: seeding date, crop cultivar characteristics, mineral and organic fertilization. The crop plant is described by its shoot dry biomass (carbon and N), LAI and biomass of harvested crop organs. The cumulative air temperature is the main input variable driving the crop growth: crop temperature is used to calculate the sum of degree-days by phenological stage. Seeding date and first phenological stages lengths have a great impact on the crop emergency date and entire LAI profile. Phenological stages are calibrated for each cultivar. One cultivar of wheat is selected (Biensur) (Brisson et al., 2002; Brisson, 1998). One cultivar of late sunflower is calibrated for STICS (Brisson et al., 2003). Water and nutrient stress indices are associated with limitations regarding leaf growth and net photosynthesis of plants. The soil water and nitrogen contents simulated at a daily time step are confronted to the daily crop requirements to compute the transpiration fluxes and nitrogen assimilation within crop biomass.

The water and N cycling in soils is explicitly detailed by simulating evaporation and transpiration, percolation to deep layers and lateral flows, organic matter mineralization, mineral nitrogen denitrification (NEMIS model; Henault and Germon, 2000; Oehler et al., 2009) and leaching into the hydrological network. The agricultural practices inputs are supplied at the crop field level: seeding date, fertilization date and amount, straw management and harvesting date.

The TNT2 hydrological module is a fully-distributed hydrological model, adapted to topography-based shallow aquifer. It is based on the hydrological model TOPMODEL assumptions (Beven, 1997): water fluxes are assumed to follow Darcy's law, with a constant hydraulic gradient. The hydraulic transmissivity depends on the soil water deficit of saturation. The main differences between TNT and TOPMODEL lie in the distribution of the recharge and the deficit of soil water saturation. TOPMODEL computes water fluxes at the outlet and an average deficit of saturation of the whole catchment, which can be distributed in each point of the basin according to a topographic index. In TNT, calculations are done following an explicit cell to cell routing. The catchment is represented by a cluster of columns. Each surface of top of column corresponds to a pixel of the Digital Elevation Model (DEM). Each height of column is divided into 2 soil layers (root growth zone) and a shallow aquifer layer. The soil and aquifer porosity is described as a dual porosity: the retention (micro) and drainage (macro) porosities. The porosity volume has to be set up for each layer, for each soil type that is spatially delineated by the soil raster map. The water flow paths are following a multi-directional scheme (a pixel can flow in several pixels), which depends directly on the surface topography calculated from the DEM. Water percolation and nitrogen leaching are computed using cascading horizontal layers similar to Burns' model (Burns, 1974), according to soil porosity characteristics. Both spatial soil characteristics and multi-directional scheme derived from DEM define a spatially explicit distribution of recharge and deficit of soil water saturation. In addition to that, cropping pattern and associated agricultural practices add spatial heterogeneity to this theoretical scheme in terms of water and nutrient transfers.

The model runs on a daily time step. Water balance and N transformations are computed in each cell of the raster grid of the DEM, from upstream to downstream by

HESSD
11, 7689–7732, 2014

following the cell-to-cell drainage routing. Daily discharge and nitrogen fluxes are computed at the outlet of the catchment.

2.5 Model calibration

The model has been calibrated for the period 1985–2001 by optimization of the daily discharge first, using both hydrological parameters To and m that influence the simulated hydrograph characteristics: To is the lateral transmissivity of the soil column at saturation (in $m^2\ day^{-1}$) and m is the exponential decay factor of the hydraulic conductivity with depth (in m). The Nash–Sutcliffe's efficiency coefficient (Nash and Sutcliffe, 1970) and RMSE were used as optimization criteria to minimize mismatching for daily discharge and nitrogen fluxes.

Using the same set of parameters than in (Ferrant et al., 2013, 2011), we evaluate the simulations for the period 2005–2010 in terms of hydrological and nitrogen fluxes, as well as evapotranspiration and LAI/biomass data that have been measured in the experimental crop field (Fig. 1).

2.6 Procedure for re-assessing seeding dates

An algorithm designed to minimize temporal shifts between simulated LAI profile and interpolated LAI profile based on satellite images at the crop field level was implemented (Fig. 2) to re-assess seeding dates at the crop field level. A first LAI profile is simulated for each crop field. As the cumulative air temperature is the main input variable driving the crop growth, the temporal shift (T_{diff}) between both simulated and interpolated LAI is estimated in cumulative temperature (in °C) for a threshold of LAI during the growth. The threshold is set to 0.7 because it avoids weed growth detection that could mislead the detection of the crop growth phase. A new seeding date is computed by subtracting the cumulative degree-day associated to the previous seeding date with T_{diff}. The obtained cumulative degree-day tends to improve the seeding date's assessment, which is used in the next iteration. Ten iterations were then performed. In

HESSD
11, 7689–7732, 2014

addition to T_{diff}, the RMSE computed for the whole set of simulated and observed LAI is used to evaluate the optimization performance. No range of variation has been predefined, as the next seeding date is computed based on the cumulative temperature differences.

3 Results

3.1 Hydrological fluxes

Drainage and nitrogen fluxes simulated for the whole catchment are compared to the measurements at the outlet. For this study, the hydrological calibration of input parameters presented in Ferrant et al. (2011) is not modified. Similar performances are found for daily discharge (Nash Sutcliffe coefficient $E = 0.4$). The annual average discharge for the period from May 2006 to December 2010 is around 71 mm yr^{-1}, which is drier than the 107 mm yr^{-1} estimated from 1985 to 2001. The simulated discharge is 88 mm yr^{1} between May 2006 and December 2010. This overestimation is comparable to that obtained for the dry years during the period 1985–2001.

Observed in-stream nitrogen fluxes from January 2007 to December 2010 are close to 7 kgN ha^{-1} yr^{-1} while simulated fluxes after LAI optimization are 9.6 kgN ha^{-1} yr^{-1} (Table 1). The simulation performance is similar to that obtained for the calibration period published by Ferrant et al. (2011). The daily simulated nitrogen loads are poorly correlated to observed data ($R^2 = 0.4$), whereas correlation of monthly loads is higher (0.6). The RMSE for monthly loads are 0.68 kgN ha^{-1}. The hydrological control on daily nitrogen loads is poorly simulated, due to the daily time step and the simplifications of the hydrological processes involved in the partition of runoff and infiltration as discussed in Ferrant et al. (2011).

HESSD
11, 7689–7732, 2014

3.2 Leaf Area Index derived from Formosat-2 images

Figure 3a shows the maps of maximal LAI for each pixel, each year and crop. Figure 3b shows the LAI spatial variability observed for the sunflower crop field in function of time: the spatial variability increases concomitantly with the crop growth. This variability, expressed as the standard deviation (sigma), is of the same order of magnitude when regarding variability between crop fields and within crop fields. Processes driving this spatial variability are mainly related to soil patterns, localization in slope or aspect of the slope. The absolute value of LAIs retrieval is compared with field measurements. Figure 4 compares different measurements of LAI: (1) RS LAI retrieved from satellite or hemispherical photographs, (2) direct measurement by destructive method. Error bars represent plus or minus one standard deviation of the median of the samples collected for destructive methods. The variability of the result is both associated to the spatial variability of LAI and biomass encountered throughout the crop field and an imprecision attributed to the measurement method itself. The LAI estimated from hemispherical photographs is an average estimate for the area covered by the camera lens; error bars represents a fixed uncertainty related to this measurement method (Demarez et al., 2008). The satellite derived LAI estimates for the crop field level is represented with the median plus or minus one standard deviation of the LAI value of each pixel located within the crop field. The error bar represents the spatial variability detected by remote sensing.

The 44 cloud free Formosat-2 images acquired in 2006 ensure a fine description of the winter wheat development. The intra-field LAI spatial variability observed with the satellite retrievals is close to 1 $m^2\,m^{-2}$ during the maturity stage. This spatial variability is estimated to be higher for the sunflower of the following year 2007 with 1.5 of LAI (Fig. 4). In 2008, the presence of clouds during the spring prevented the observation of the winter wheat growth, whereas images taken during the summer allowed surveying the sunflowers growth. These results illustrate the intrinsic accuracy of each measurement method, and the spatio-temporal variability of the crop growth. The F2 spatial resolution and high revisit frequency allow us to capture the growth dynamics.

3.3 Optimizing LAI profile

Figure 5 shows the results of the optimization of the temporal dynamics of the LAI average over the 101 crop fields. The reinitializing of the seeding dates decreases the temporal shift (Tdiff) by 7 times in average. The optimized simulated LAI profiles match better with the observed data for each wheat growing period. The differences for the sunflower are small since the temporal shift between interpolated observations and simulated LAI were already small. This indicates that the first-guess seeding dates of the sunflower were accurate. A slight decrease of RMSE is observed after optimization, meaning that this estimator is not sensitive to the seeding date re-assessment. Indeed, the RMSE value is representative of the whole LAI series, whereas the optimization process only takes the early phenological stages into account. Furthermore, senescence stage of the winter wheat is not appropriately simulated: after the maximum is reached, simulated LAI remain stable until the harvest. The observed LAI from satellite are derived from photosynthesis activity which decrease early when the wheat get dry. This part of the development is better described in last released of STICS 6. The trajectories of seeding date solutions in function of the iteration number (Fig. 6) show a quick convergence after 5 iterations. There are few crop fields for which no realistic solutions are found. For the sunflower 2007, 4 crop fields converged to early seeding date in October to December. This concerns exclusively the sunflower in some small crop fields (few hectares) for which average LAI remain low (<). In these cases, the maximum of observed LAI is too low or the proportion of mixed pixels (at the crop field border) is too high leading thus to unrealistic interpolations of the LAI profile at the crop field level. The annual seeding dates estimated by this method are comprised in a large period for the winter wheat and short for the sunflower. These ranges are from September to the beginning of November for winter wheat and between January to April (highly depending on the climatic year) for the sunflower.

HESSD
11, 7689–7732, 2014

3.4 Sensitivity of discharge and stream nitrogen fluxes to seeding date

Table 1 presents the annual water and nitrogen fluxes computed for the whole simulation period (2006–2010). The changes in crop development induced by the re-initialization of input parameters have a small effect on the discharge and AET (around 1 to 2 mm yr^{-1}). On the contrary, the global nitrogen uptake by the crop is increased in the case of seeding date re-initializing (+3 kgN ha^{-1} yr^{-1}). This leads to a decrease of in-stream nitrogen fluxes at the outlet to 9.6 kgN ha^{-1} yr^{-1}, which is closer to the annual N fluxes measured at the outlet (7.5 kgN ha^{-1} yr^{-1}). The yields of wheat crops are more impacted by the seeding date re-initialization than the sunflower (Fig. 5); actually, the wheat yield increases from 5 to 5.8 t ha^{-1} whereas it remains stable for the sunflower. This optimization process has increased the Nitrogen Use Efficiency (NUE) of wheat as well. This ratio of nitrogen uptake by the plant and nitrogen input by fertilizers aims at identifying the agricultural practices efficiency. It means that the N inputs from fertilization are better absorbed by the plants. Nevertheless the N content in grain ratio is slightly decreased since it depends on both grain biomass and N content in grain. The sunflower yield is not impacted since the LAI profiles have not been really modified by the re-initializing of the seeding date.

3.5 Impact at a crop field level

Figure 7 shows the results of seeding date re-initialization respectively on the LAI and biomass estimates. We compare two crop fields, one is located within the catchment where TNT2 simulation are performed (crop field 8) and the second is the experimental crop field where atmospheric turbulent fluxes measurements are located (see Fig. 1). The crop fields are close to each other and comparable in terms of slopes and crop rotation, except for 2009 when rapeseed crop was grown at the experimental field, whereas a sunflower was sown in the crop field 8 located within the catchment. Remotely-sensed LAI values for both crop fields are compared to illustrate the differences observed between both crops in term of vegetation dynamics. The interpolated

HESSD
11, 7689–7732, 2014

daily LAI is presented in Fig. 7 for the crop within the catchment, and both simulated LAI profile before and after the optimization are plotted. The simulated biomass before and after the optimization in the crop field 8 are compared to the measured biomass within the experimental crop field. The spatio-temporal variability of this variable is close to the measurements for the 4 years, except in 2008 where no optimization could be performed due to cloud laden condition. The seeding date modifications have a substantial impact on the biomass production and improve clearly the biomass predictions in 2010.

The Fig. 8 compares the daily simulated and measured evapotranspiration fluxes at respectively the crop field 8 and experimental crop field level. Each series are highly correlated in time ($R > 0.7$) which means that the climatic control of the AET is conveniently accounted for. On the contrary, the Nash Sutcliffe coefficient E, usually used for hydrological fluxes evaluation, exhibits high inter-annual variability, from a good correspondence between flux measurements and simulations in 2006 ($E = 0.57$) to negative value in the 2007, 2008 and 2010 years. It shows that bias is high; cumulative annual measured AET tends to be overestimated by simulations, by 11 and 15 % in 2006 and 2007, and by more than 30 % in 2008 and 2010. The RMSE of each series is around 1 mm day^{-1} except for the year 2006 for which it is twice as less. Figure 8 shows the uncertainty associated to the random measurement errors for semi-hour fluxes as an envelope around the daily AET, and indicates that it is roughly proportional to the flux intensity (Béziat et al., 2009). Eddy covariance measurements are representative of a fluctuating area (called footprint) of the crop field which varies mainly with the crop cover height as well as wind speed and direction. The footprint, corresponding to the area which is contributing to the measurements made at the tower location, has been computed in a previous non published study using both half hourly climatic variables locally measured and a footprint model (Horst, 1999). Figure 8 (right part) represents the average footprint area for the years 2006, 2007 and 2008 estimated by the footprint model, climatic data and crop height measured in the experimental crop field. It shows the total contributive area and the location of high contributive area (colors in yellow and red). Two main wind directions explain the footprint symmetry on both sides of an

HESSD
11, 7689–7732, 2014

NNE–SSW axe. The main contributive area remains close to the flux tower; the footprint in 2006 is more homogeneous and large than those in 2007 and 2008. Average footprint areas are close to the flux tower, which is not representative of the entire experimental crop field; furthermore the footprint area is located in a zone characterized by low soil depth associated to low crop productivity. These AET measurements may therefore represent a low boundary of the AET range within the plot. TNT2 estimates at the crop field (8) level are systematically higher than the in-field measurements, but the spatial variability within the crop field (represented by whiskers of standard deviation each 10 days) is comprised between 0.4 to 1.8 mm day^{-1} during the crop growing season (spring and summer). This spatial variability is as high as the RMSE found for both observed and simulated series. Unfortunately, comparison between observed and simulated AET cannot be done for the footprint area only as the crop fields are distant by 800 m from each other.

4 Discussion

4.1 About LAI profile improvement

Field measurements of LAI or AET are expensive and time-consuming, and are limited to local evaluations of the crop cover. The satellite observations are then essential to monitor the crop cover dynamics at crop field scales. In the study context, high spatial variability of this biophysical variable is observed, which makes high spatial resolution of retrieved LAI interesting to map the spatial variability of crop productivity. We identify that the LAI maps derived from F2 series provide an accurate estimate of the LAI profiles variability in space and time. The large number of images, provided by a high frequency of satellite revisit, makes it possible to describe the temporal crop development and productivity at pixel and crop field levels by describing the LAI profile retrieved from F2 images with a physically based double logistic descriptive equation (Fig. 2). This temporal information has been used at the crop field level to optimize the simulated

LAI of the process-based model STICS, coupled with a hydrological model that aim at varying local situations described by hydrological conditions within the catchment. The objectives of minimizing the temporal shift between measured and observed LAI by re-initializing seeding date in TNT2 is satisfactorily fulfilled with a quick convergence of the optimization process; temporal shifts are generally minimized with a realistic seeding date solution.

4.2 About seeding date estimation

Nevertheless, even if seeding date values are a good numerical solution for phasing simulated and RS retrieved LAI profile, final seeding date values mainly depend on the cultivar parameters, such as length of early development stage and vernalisation stage. For instance, winter wheat vernalisation duration, corresponding to low temperature periods requirements to hasten plant development, will depend on a number of vernalising days defined for each wheat cultivar (JVC parameter) and the crop temperature computed from climate input data. The mild winter conditions in the study area make the LAI profile insensitive to the seeding date for high value of JVC (> 8). Therefore, we have set the JVC parameter to 6 days for the winter wheat cultivar used in this study. This shows that the wheat variety is crucial information for a better estimation of the true seeding date, crop growth dynamic and yield elaboration.

4.3 About the optimization process performance

Jégo et al. (2012) used LAI data retrieved from satellite images to better constrain input parameters of the STICS crop model. By re-initialization of the seeding date, they greatly improved the model predictions in terms of biomass and yield. The optimization method is based on the simplex algorithm to minimize the weighted sum of squared differences between RS retrieved and simulated LAI series. A run of the crop model is done for one crop and one year, and lasts less than a second. This optimization method is appropriate since it tests several input parameter couples to converge quickly to an optimal solution in terms of the chosen estimator. In the case of TNT2, simulations are sequentially executed: each pixel calculation depends on previous and neighborhood simulated conditions. One run corresponds to the simulation of water and nutrient fluxes in 134 013 modeling units, corresponding to 101 crop fields for 5 years. Hence, it requires much more computation times (around 2 h for the Montoussé river catchment). The hydrological interactions between modeling units in space and time imply that changes in seeding dates are inter-dependant. The optimization method described in this paper was chosen because it is based on a quantitative estimator (rather than statistical estimator) of the temporal shifts which is used to correct quantitatively the input parameter (here the seeding date) based on the model functioning. Indeed, the temporal delay between RS retrieved and simulated LAI series is evaluated as a physical variable: the cumulative daily air temperature difference. The results of this optimization show a quick convergence after 5 to 8 iterations.

4.4 About the impact of re-initializing on agro-hydrological variables

TICS crop model (agronomical part of the TNT2 model) is a process-based model, i.e. it is able to scale up the results of local experiments. It extrapolates the crop growth variables from analogous situations described by input data (soil, climatic and cropping management), without the need for new testing. The coupling of this process-based model with a hydrological model aims at simulating varying local situations described by hydrological conditions within the catchment: saturated zones, soil water content in function of the situation within slope. The hydrological variables -evapotranspiration and discharge –are not heavily impacted by this change in crop cover dynamics. The difference obtained for AET, i.e. 2 $\mathrm{mm\,yr^{-1}}$, is similar to the impact of cover crop tested in this catchment using TNT2 for the period 1985–2001 (Ferrant et al., 2013). On the contrary, the improvement of the crop cover dynamics representation obtained by the seeding date re-initializing has a substantial impact on wheat biomass production (Fig. 7) and associated nitrogen uptake: NUE and yield of winter wheat are mainly increased by the re-initializing process. Thus, simulated nitrogen fluxes into the environment

HESSD
11, 7689–7732, 2014

decreases by 2.7 and 11.9 % for respectively denitrification and stream losses. Dynamically controlled by the discharge, in-stream nitrogen fluxes simulated during a long period highly depend on the balance between fertilizer applications and crop consumption. In that case, average annual simulated nitrogen fluxes have been decreased from 11 to 9.6 $\mathrm{kgN\,ha^{-1}\,yr^{-1}}$ which is in better agreement with the 7.5 $\mathrm{kgN\,ha^{-1}}$ annual estimation based on intensive measurements. In general, the improvement of the spatial and temporal crop cover and nitrogen uptake representation would benefit to the understanding of the N cycle by estimating the nitrogen excess location and the associated potential losses into hydrologic or atmospheric system. The mapping of the NUE in 2007 is presented in Fig. 10. As a ratio between nitrogen fertilizer input(crop field level) and the plant uptake (at the pixel size), it indicates the areas where plant uptakes exceeds N inputs (NUE $>$ 1) and the areas contributive to N losses where N inputs exceed plant uptake (NUE $<$ 1). These representations of the nitrogen excess in the landscape will definitely benefit from a crop development optimization at the pixel level using LAI derived from RS images series.

4.5 About other input parameter (soil and hydromorphy) and spatial representation of hydrological situations

Other input parameters than seeding date should be considered for further optimizations. Indeed, Jégo et al. (2012) identify a second input parameter known to have a great impact on crop productivity within STICS crop model: the soil water-holding capacity. In TNT2 model, the soil map defines homogeneous zones where 21 soil parameters are defined. The sensitivity of the spatial pattern of soil input parameters within agro-hydrological models is not yet deeply explored. Figure 8 shows the spatial variability of the F2 derived and TNT2 simulated LAI at the pixel level for two dates. Two covariates seem to drive the spatial variability of the LAI variations simulated by TNT2: the soil map and the drainage network location. Three main situations are simulated: (1) systematic saturated conditions that limit the LAI development in the drainage network location (2) low soil water deficit that enhances LAI development, (3) intermediate or low soil water content that limits the LAI development. There is a high potential of agronomical calibration of agro-hydrological models by reinitializing soil input parameters and refining local situations at the pixel size, using these newly LAI map series derived from optical RS with high revisit frequency. Considering only hydrological variables, Moreau et al. (2013) have tested the sensitivity of the TNT2 model response to spatial soil input parameters map for both water and nitrogen related parameters. They analyzed the output sensitivity in term of in-stream water and nitrogen fluxes at the outlet and concluded that sensitivity to spatial distribution of soil input factors is low. Beyond this perspective, we consider that the sensitivity of spatial soil input parameters is high on crop variables and would impact the spatial representation of N cycle within slopes. The re-initialization of the soil physical parameters of the TNT2 model will be proposed in a forthcoming study at the pixel level, using the same F2 dataset. The control of these parameters against other catchment physical parameters (aspect, slopes...) on the spatial and temporal variability of the crop growth will be explored.

5 Conclusions

The present study evaluated the potential of remote sensing data series for spatial and temporal calibration of a distributed agro-hydrological model for 5 years (2006–2010). The use of a physical knowledge based crop model (STICS) coupled with a simplified hydrological model (TNT) gives the opportunity to simulate the water and nitrogen budget as well as yields of a soil-plant system at the catchment scale, taking climatic and agricultural variables into account. The lack of spatial and temporal calibration of soil-crop situations is assessed regarding to the additional spatio-temporal information derived from RS images. The spatial calibration of model input parameters, previously fixed to a priori values, using LAI derived from RS images series gives new opportunities to constrain the spatial and temporal crop development at the catchment scale. In this example, we satisfactorily constrained the temporal LAI development at the crop field level by re-initializing the seeding date. This calibration step adds value to the conventional calibration process usually performed for agro-hydrological model. The better representation of the crop cover growth has no noticeable impact on the water budget at the catchment scale (around 1 %), but had substancial impacts on nitrogen cycle in terms of crop uptake and biomass as well as nitrate leaching and in-stream losses. The optimization process using RS derived LAI profile has allowed increasing the nitrogen uptake by the crop and the biomass production for the winter wheat, leading to a non negligible drop of the simulated in-stream nitrogen losses by around 12 %. This result indicates that a spatial calibration of the crop biophysical variables such as LAI changes the N use efficiency (NUE) at the crop field level which impacts the nitrogen cycle at the catchment scale.

This study demonstrates the contribution of high spatial resolution optical satellite images with frequent systematic observation in spatial calibration of agro-hydrological model. This type of spatial calibration greatly improve the capacities of agro-hydrological modeling to explain, reproduce and predict spatial crop growth by constraining the spatial water and nutrient fluxes within hydrological catchment. Massive systematic satellite observations will be widely available thanks to forthcoming satellite missions Venμs (Dedieu et al., 2006) and Sentinel-2 that will provide high spatial resolution images with 4/5 days of revisiting period. Further development will test a similar re-initialization algorithm on main soil parameters controlling soil water content to improve the simulated LAI profile at pixels level.

References

Arnold, J. G., Allen, P. M., and Bernhardt, G.: A comprehensive surfacegroundwater flow model, J. Hydrol., 142, 47–69, 1993.

Arnold, J. G., Srinivasan, R., Muttiah, R. S., and Williams, J. R.: Large-area hydrologic modeling and assessment: Part I. Model development, J. Am. Water Ressour. Assoc., 34, 73–89, 1998.

Baldocchi, D., Hicks, B., and Meyers, T.: Measuring biosphere–atmosphere exchanges of biologically related gases with micrometeorological methods, Ecology, 69, 1331–1340, 1988.

Baret, F., Hagolle, O., Geiger, B., Bicheron, P., Miras, B., Huc, M., Berthelot, B., Nino, F., Weiss, M., Samain, O., Roujean, J. L., and Leroy, M.: LAI, fAPAR and fCover CYCLOPES global products derived from VEGETATION, Part 1: Principles of the algorithm, Remote Sens. Environ., 3, 275–286, 2007.

Baret, F., De Solan, B., Lopez-Lozano, R., Ma, K., and Weiss, M.: GAI estimates of row crops from downward looking digital photos taken perpendicular to rows at 57.5 degrees zenith angle: theoretical considerations based on 3D architecture models and application to wheat crops, Agr. Forest Meteorol., 150, 1393–1401, 2010.

Beaujouan, V., Durand, P., Ruiz, L., Aurousseau, P., and Cotteret, G.: A hydrological model dedicated to topography-based simulation of nitrogen transfer and transformation: rationale and application to the geomorphology-denitrification relationship, Hydrol. Process., 16, 493–507, 2002.

Beven, K: Distributed modelling in hydrology: applications of topmodel concept, Adv. Hydrol. Process., 350, 1997.

Beven, K: Equifinality, data assimilation, and uncertainty estimation in mechanistic modelling of complex environmental systems using the glue methodology, J. Hydrol., 249, 11–29, doi:10.1016/S0022-1694(01)00421-8, 2001.

Béziat, P., Ceschia, E., and Dedieu, G.: Carbon balance of three crop succession over two cropland sites in South West of France, Agr. Forest Meteorol., 149, 1628–1645, 2009.

Birkinshaw, S. and Ewen, J.: Nitrogen transformation component for Shetran catchment nitrate transport modelling, J. Hydrol., 230, 1–17, 2000.

Bosch, N. S: The influence of impoundments on riverine nutrient transport: an evaluation using the soil and water assessment tool, J. Hydrol., 355, 185–193, 2008.

Breuer, L., Vaché, K., and Julich, S. H.-G. F.: Current concepts in nitrogen dynamics for mesoscale catchments, Hydrolog. Sci. J., 53, 1059–1074, doi:10.1623/hysj.53.5.1059, 2008.

Brisson, N., Mary, B., Ripoche, D., Jeuffroy, M. H., Ruget, F., Nicoullaud, B., Gate, P., Devienne-Barret, F., Antonioletti, R., Durr, C., Richard, G., Beaudoin, N., Recous, S., Tayot, X., Plenet, D., Cellier, P., Machet, J.-M., Meynard, J. M., and Delécolle, R.: Stics: a generic model for the simulation of crops and their water and nitrogen balances, I. Theory and parameterization applied to wheat and corn, Agronomie, 18, 311–346, 1998.

HESSD
11, 7689–7732, 2014

Agro-hydrology and multi temporal high resolution remote sensing

S. Ferrant et al.

Brisson, N., Ruget, F., Gate, P., Lorgeou, J., Nicoullaud, B., Tayot, X., Plenet, D., Jeuffroy, M. H., Bouthier, A., Ripoche, D., Mary, B., and Justes, E.: STICS: a generic model for simulating crops and their water and nitrogen balances, II. Model validation for wheat and maize, Agronomie, 22, 69–92, 2002.

Brisson, N., Gary, C., Justes, E., Roche, R., Mary, B., Ripoche, D., Zimmer, D., Sierra, J., Bertuzzi, P., Burger, P., Bussière, F., Cabidoche, Y. M., Cellier, P., Debaeke, P., Gaudillère, J. P., Hénault, C., Maraux, F., Seguin, B., and Sinoquet, H.: An overview of the crop model STICS, Eur. J. Agron., 18, 309–332, 2003.

Brocca, L., Melone, F., Moramarco, T., and Morbidelli, R.: Antecedent wetness conditions based on ERS scatterometer data, J. Hydrol., 364, 73–87, 2009.

Brocca, L., Moramarco, T., Melone, F., Wagner, W., Hasenauer, S., and Hahn, S.: Assimilation of Surface- and Root-Zone ASCAT Soil Moisture Products Into Rainfall–Runoff Modeling, IEEE T. Geosci. Remote, 50, 2542–2555, 2012.

Burns, I: A model for predicting the redistribution of salts applied to fallow soils after excess of rainfall or evaporation, J. Soil Sci., 25, 165–178, 1974.

Cheema, M. J. M., Immerzeel, W. W., and Bastiaanssen, W.: Spatial quantification of groundwater abstraction in the irrigated Indus basin, Groundwater, 52, 25–36, 2014.

Chen, J. M., Chen, X., Ju, W., and Geng, X.: Distributed hydrological model for mapping evapotranspiration using remote sensing inputs, J. Hydrol., 305, 15–39, 2005.

Chern, J. S., Wu, A. M., and Lin, S. F.: Lesson learned from Formosat-2 mission operations, Acta Astronaut., 59, 344–350, 2006.

Claverie, M.: Estimation spatialisée de la biomasse et des besoins en eau des cultures à l'aide de données satellitales à hautes résolutions spatiale et temporelle: application aux agrosystèmes du Sud-Ouest de la France, Université de Toulouse, Toulouse, 2012.

Claverie, M., Vermote, E. F., Weiss, M., Baret, F., Hagolle, O., and Demarez, V.: Validation of coarse spatial resolution LAI and FAPAR time series over cropland in southwest France, Remote Sens. Environ., 139, 216–230, 2013.

Demarez, V., Duthoit, S., Baret, F., Weiss, M., and Dedieu, G.: Estimation of leaf area and clumping indexes of crops with hemispherical photographs, Agr. Forest Meteorol., 148, 644–655, 2008.

Duchemin, B., Maisongrande, P., Boulet, G., and Benhadj, I.: A simple algorithm for yield estimates: evaluation for semi-arid irrigated winter wheat monitored with green leaf area index, Environ. Model. Softw., 23, 876–892, 2008.

HESSD

11, 7689–7732, 2014

Agro-hydrology and multi temporal high resolution remote sensing

S. Ferrant et al.

Durand, P.: Simulating nitrogen budgets in complex farming systems using INCA: calibration and scenario analyses for the Kervidy catchment (W. France), Hydrol. Earth Syst. Sci., 8, 793–802, doi:10.5194/hess-8-793-2004, 2004.
Engel, B. A., Shrinivasan, R., Arnold, J. G., Rewerts, C., and Brown, S. J.: Nonpoint source (NPS) pollution modeling using models integrated with Geographic Information Systems (GIS), Water Sci. Technol., 28, 685–690, 1993.
Ferrant, S: Modélisation agro-hydrologique des transferts de nitrates à l'échelle des bassins versants agricoles gascons, Atelier national de reproduction des thèses, Lille, 2009.
Ferrant, S., Oehler, F., Durand, P., Ruiz, L., Salmon-Monviola, J., Justes, E., Dugast, P., Probst, A., Probst, J. L., and Sanchez-Perez, J. M.: Understanding nitrogen transfer dynamics in a small agricultural catchment: comparison of a distributed (TNT2) and a semi distributed (SWAT) modelling approaches, J. Hydrol., 406, 1–15, 2011.
Ferrant, S., Laplanche, C., Durbe, G., Probst, A., Dugast, P., Durand, P., Sanchez-Perez, J. M., and Probst, J. L.: Continuous measurement of nitrate concentration in a highly event-responsive agricultural catchment in south-west of France: is the gain of information useful?, Hydrol. Process., 27, 1751–1763, doi:10.1002/hyp.9324, 2012.
Ferrant, S., Durand, P., Justes, E., Probst, J. L., and Sanchez-Perez, J. M.: Simulating the long term impact of nitrogen scenarios in a small agricultural catchment, Agr. Water Manage., 124, 85–96, 2013.
Ferrant, S., Caballero, Y., Perrin, J., Gascoin, S., Dewandel, B., Aulong, S., Dazin, F., Ahmed, S., and Maréchal, J. C.: Projected impacts of climate change on farmers' extraction of groundwater from crystalline aquifers in South India, Scientific Report 4, doi:10.1038/srep03697, 2014.
Franczyk, J. and Chang, H.: The effects of climate change and urbanization on the runoff of the Rock Creek basin in the Portland metropolitan area, Oregon, USA, Hydrol. Process., 23, 805–815, 2009.
Galloway, J. N., Aber, J. D., Erisman, J. W., Seitzinger, S. P., Howarth, R. W., Cowling, E. B., and Cosby, B. J.: The nitrogen cascade, Bioscience, 53, 341–356, 2003.
Hagolle, O., Dedieu, G., Mougenot, B., Debaeker, V., Duchemin, B., and Meygret, A.: Correction of aerosol effects on multi-temporal images acquired with constant viewing angles: application to Formoat-2 images, Remote Sens. Environ., 112, 1689–1701, 2008.

HESSD
11, 7689–7732, 2014

Agro-hydrology and multi temporal high resolution remote sensing

S. Ferrant et al.

Hagolle, O., Huc, M., Pascual, D. V., and Dedieu, G.: A multi-temporal method for cloud detection, applied to FORMOSAT-2, VENuS, LANDSAT and SENTINEL-2 images, Remote Sens. Environ., 114, 1747–1755, 2010.
Henault, C. and Germon, J. C.: NEMIS, a predictive model of denitrification on the field scale, Eur. J. Soil Sci., 51, 257–270, 2000.
Horst, T: The footprint for estimation of atmosphere–surface exchange fluxes by profile techniques, Bound.-Lay. Meteorol., 90, 171–188, 1999.
Hutchings, N. J., Reinds, G. J., Leip, A., Wattenbach, M., Bienkowski, J. F., Dalgaard, T., Dragosits, U., Drouet, J. L., Durand, P., Maury, O., and de Vries, W.: A model for simulating the timelines of field operations at a European scale for use in complex dynamic models, Biogeosciences, 9, 4487–4496, doi:10.5194/bg-9-4487-2012, 2012.
Immerzeel, W. W. and Droogers, P.: Calibration of a distributed hydrological model based on satellite evapotranspiration, J. Hydrol., 349, 411–424, 2008.
Immerzeel, W. W., Gaur, A., and Zwart, S. J.: Integrating remote sensing and a process-based hydrological model to evaluate water use and productivity in south Indian catchment, Agr. Water Manage., 95, 11–24, 2008.
Jacquemoud, S., Verhoef, W., Baret, F., Bacour, C., Zarco-Tejada, P. J., Asner, G. P., François, C., and Ustin, S. L.: PROSPECT + SAIL models: a review of use for vegetation characterization, Remote Sens. Environ., 113, 56–66, 2009.
Jégo, G., Pattey, E., and Liu, J..: Using Leaf Area Index, retrieved from optical imagery, in the STICS crop model for predicting yield and biomass of field crops, Field Crop. Res., 131, 63–74, 2012.
Laguardia, G. and Niemeyer, S.: On the comparison between the LISFLOOD modelled and the ERS/SCAT derived soil moisture estimates, Hydrol. Earth Syst. Sci., 12, 1339–1351, doi:10.5194/hess-12-1339-2008, 2008.
Laurent, F., Ruelland, D., and Chapdelaine, M.: The effectiveness of changesin agricultural practices on water quality as simulated by the SWATmodel, J. Water Sci., 20, 395–408, 2007.
Ledoux, E., Gomez, E., Monget, J. M., Viavattene, C., Viennot, P., Ducharne, A., Benoit, M., Mignolet, C., Schott, C., and Mary, B.: Agriculture and groundwater nitrate contamination in the Seine basin, The STICS-MODCOU modelling chain, Sci. Total Environ., 375, 33–47, 2007.

HESSD
11, 7689–7732, 2014

Agro-hydrology and multi temporal high resolution remote sensing

S. Ferrant et al.

Leonard, R. A., Knisel, W. G., and Still, W. G.: GLEAMS: groundwater loading effects of agricultural management systems, T. ASAE, 30, 1403–1418, 1987.
Liu, S., Tucker, P., Mansell, M., and Hursthouse, A.: Development and application of a catchment scale diffuse nitrate modelling tool, Hydrol. Process., 19, 2625–2639, 2005.
Liu, S., Mo, X., Zhao, W., Naeimi, V., Dai, D., Shu, C., and Mao, L.: Temporal variation of soil moisture over the Wuding River basin assessed with an eco-hydrological model, in-situ observations and remote sensing, Hydrol. Earth Syst. Sci., 13, 1375–1398, doi:10.5194/hess-13-1375-2009, 2009.
Lunn, R., Adams, R., Mackay, R., and Dunn, S.: Development and application of a nitrogen modelling system for large scale catchments, J. Hydrol., 174, 285–304, 1996.
Moreau, P: Modélisation intégrée des systèmes agricoles et de la dynamique de l'azote dans le bassin versant: de la conception du modèle au test de scénarios, Université Européenne de Bretagne, Rennes, 2012.
Moreau, P., Viaud, V., Parnaudeau, V., Salmon-Monviola, J., and Durand, P.: An approach for global sensitivity analysis of a complex environmental model to spatial inputs and parameters: a case study of an agro-hydrological model, Environ. Model. Softw., 47, 74–87, 2013.
Nagler, P: The role of remote sensing observations and models in hydrology: the science of evapotranspiration, Hydrol. Process., 25, 3977–3978, 2011.
Oehler, F., Durand, P., Bordenave, P., Saadi, Z., and Salmon-Monviola, J.: Modelling denitrification at the catchment scale, Sci. Total Environ., 407, 1726–1737, 2009.
Perrin, J., Ferrant, S., Massuel, S., Dewandel, B., Marechal, J. C., Aulong, S., and Ahmed, S.: Assessing water availability in a semi-arid watershed of southern India using a semi-distributed model, J. Hydrol., 460–461, 143–155, 2012.
Refsgaard, J., Thorsen, M., Jensen, J., LKleeschulte, S., and Hansen, S.: Large scale modelling of groundwater contamination from nitrate leaching, J. Hydrol., 211, 117–140, 1999.
Reiche, E: Modelling water and nitrogen dynamics on a catchment scale, Ecol. Model., 75–76, 371–384, 1994.
Taghvaeian, S. and Neale, C. M. U.: Water balance of irrigated areas: a remote sensing approach, Hydrol. Process., 25, 4132–4141, 2011.
Tallec, T., Béziat, P., Jarosz, N., Rivalland, V., and Ceschia, E.: Crop's water use efficiencies in temperate climate: comparison of stand, ecosystem and agronomical approaches, Agr. Forest Meteorol., 168, 69–81, 2013.

Volk, M., Liersch, S., and Schmidt, G.: Towards the implementation of the European water framework directive? Lessons learned from water quality simulations in an agricultural watershed, Land Use Policy, 26, 580–588, 2009.

Wagner, W., Verhoest, N. E. C., Ludwig, R., and Tedesco, M.: Editorial "Remote sensing in hydrological sciences", Hydrol. Earth Syst. Sci., 13, 813–817, doi:10.5194/hess-13-813-2009, 2009.

Whitehead, P., Wilson, E., and Butterfield, D.: A semi-distributed integrated nitrogen model for multiple source assessment in catchment, Part 1. Model structure and process equations, Sci. Total Environ., 210/211, 547–558, 1998.

HESSD

11, 7689–7732, 2014

Agro-hydrology and multi temporal high resolution remote sensing

S. Ferrant et al.

Table 1. Yearly water and N balance simulated in TNT2 model, for a priori and re-set seeding date.

TNT2 (2006–2010)	A priori seeding date	After LAI optimization
Water budget in mm yr^{-1}		
Actual ET	574	575
Rainfall	665	665
Discharge	88.5	86.7
Δ stock aquifer/soil	+2.5	+3.3
Mineral nitrogen budget kg N ha^{-1} yr^{-1}		
Mineral fertilizer	91.5	91.5
Fertilizer volatilization	1.8	1.8
Mineralization	63	62.5
Plant uptake	105.6	108
Denitrification	32.6	31.7
Stream losses	10.9	9.6
Δ stock N in the basin	+3.6	+2.9
Winter Wheat		
yield t ha^{-1} of wheat	5.0	5.8
N content in grain g kg^{-1}	22.5	20.9
NUE	0.68	0.76
Sunflower		
yield t ha^{-1} of sunflower	1.7	1.7
N content in grain g kg^{-1}	38.3	38.2
NUE	1.07	1.07

HESSD
11, 7689–7732, 2014

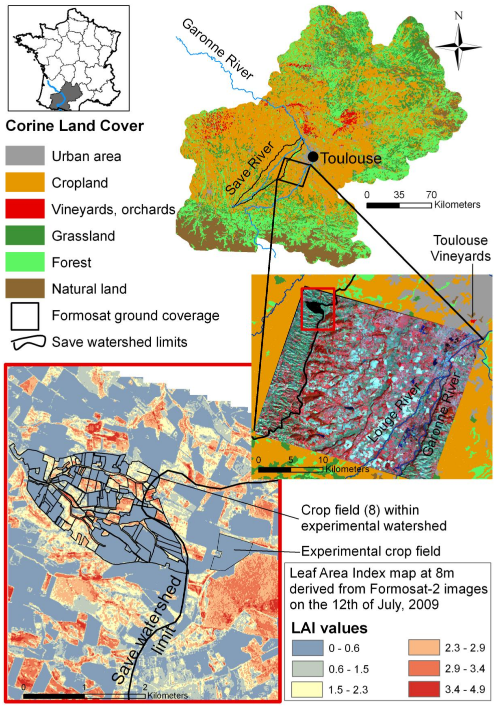

Figure 1. Situation of the studied area catchment. The Auradé catchment is constituted by 101 cultivated crop fields. The cropping pattern is a rotation of winter wheat and sunflower. The Formosat-2 series ground coverage is representative of the cropland area characterizing the surrounding region of Toulouse. Atmospheric turbulent fluxes, ground vegetation dynamic and agro-meteorological measurements are performed in the experimental crop field nearby the study site since 2005. A detail of the LAI map derived from the Formosat-2 image for the 12 July 2009 show a high variability of the LAI within the sunflower plots (still active at this period of the year), whereas other parts close to zero correspond to the winter wheat after having reached senescence stage.

HESSD
11, 7689–7732, 2014

Agro-hydrology and multi temporal high resolution remote sensing

S. Ferrant et al.

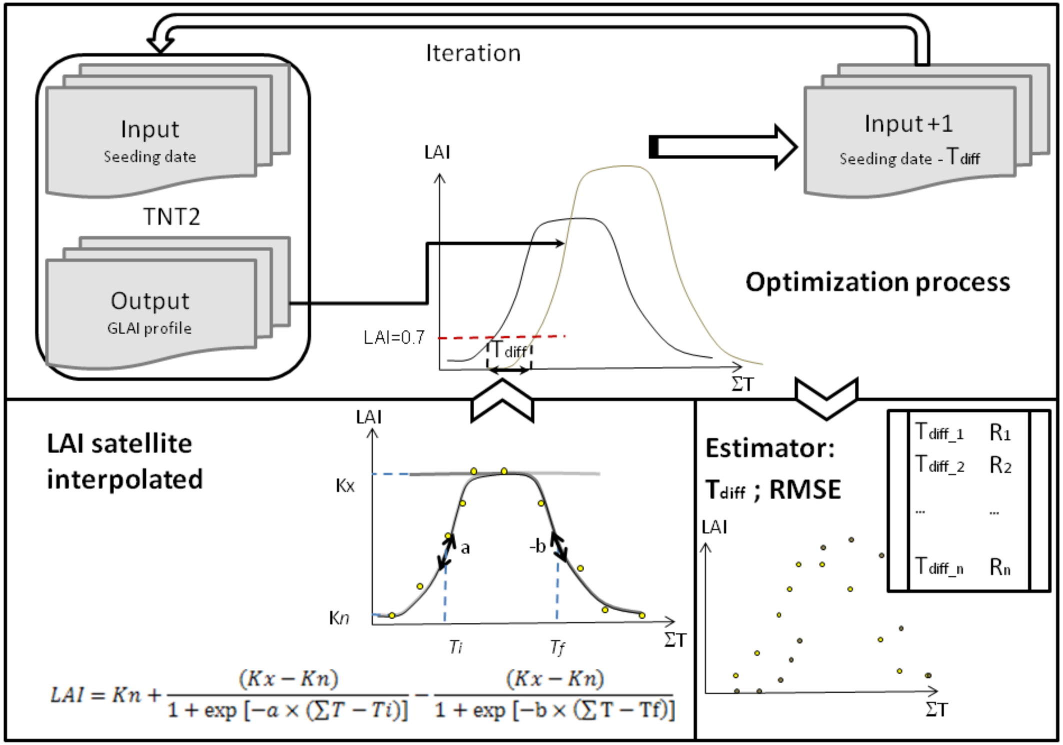

Figure 2. Optimization scheme of the seeding date by matching the early variations of simulated LAI with the interpolated GAI derived from F2 images series at the crop field scale. The interpolated GAI are obtained by fitting a double logistic equation against discrete satellite-derived LAI at the crop field scale.

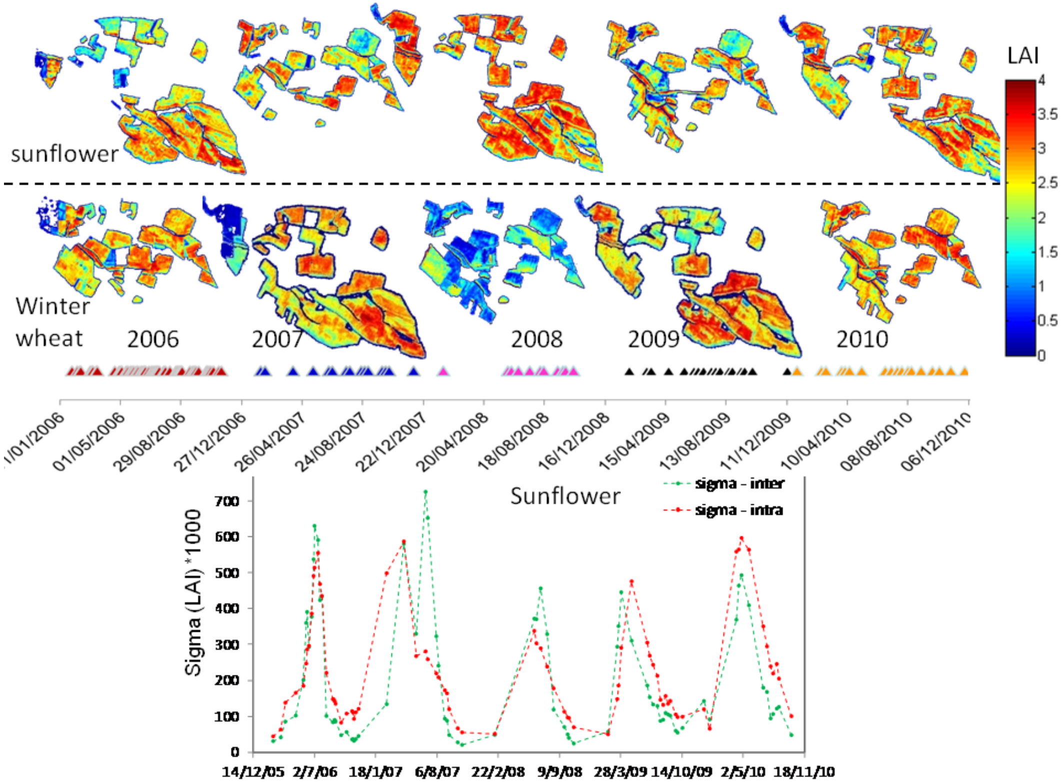

Figure 3. Top panel: maps of maximum of LAI observed for each year and each crop mask. Maximum of winter wheat LAI are not observed during the spring 2008 due to clouds covering the whole area. Each date of image acquisition constituting the F2 series is reported by a triangle in the timeline. Bottom panel: the spatial variability of the LAI in function of the time between (inter-sigma) and within (intra-sigma) crop field for the sunflower.

HESSD
11, 7689–7732, 2014

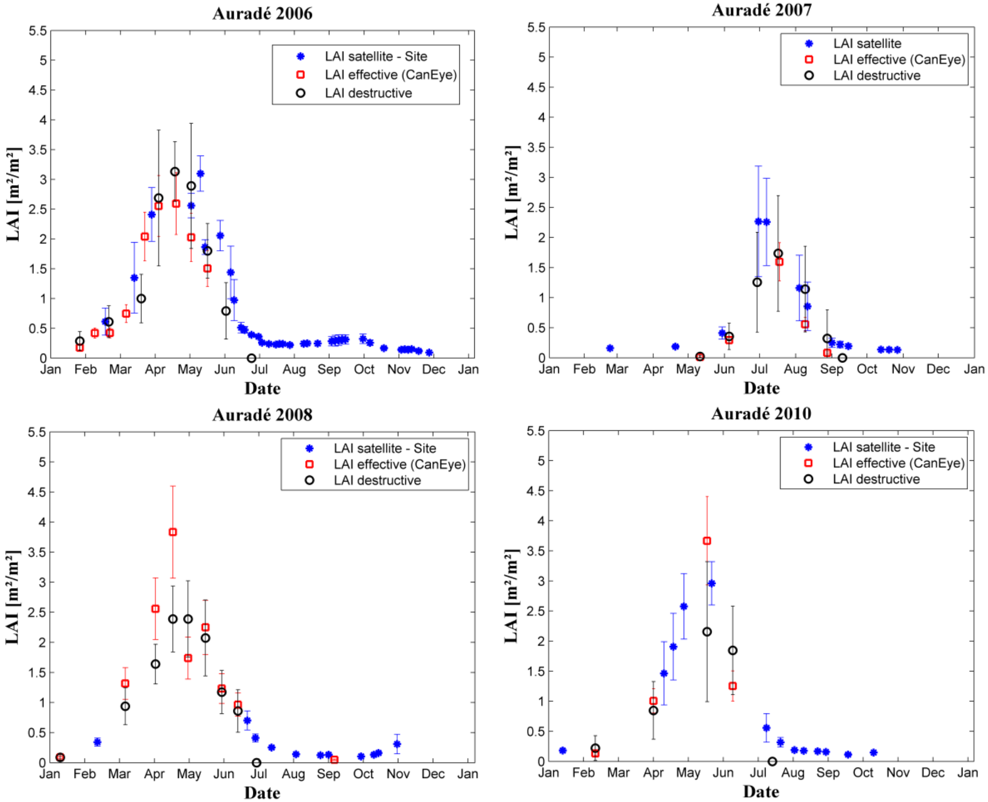

Figure 4. Leaf Area Index derived from satellite F2 images, hemispherical photographs (LAI effective CanEye) and direct field measurement (LAI destructive) in the experimental crop field located near Auradé catchment (see location in Fig. 1). The standard deviation represents the spatial variability within the crop field (LAI satellite), both spatial variability and associated sampling error (LAI destructive), uncertainty around the photo interpretation (LAI effective).

HESSD
11, 7689–7732, 2014

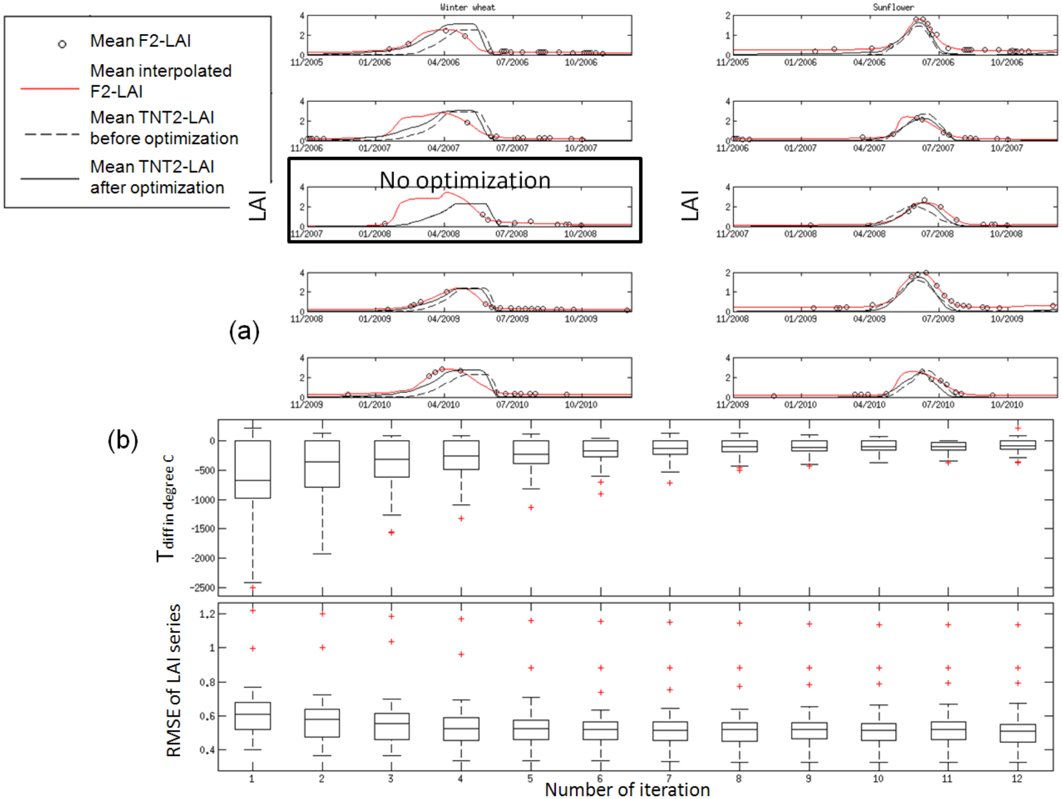

Figure 5. (a) Average LAI computed at the crop field level for the winter wheat (left panel) and sunflower (right panels) for each year of simulation (lines). Simulated LAI before and after the optimization process are respectively in dotted and full black line. Average crop field level LAI retrieved from F2 images are represented by black circle and the average interpolation from these images are in full red line. **(b)** Evolution of T_{diff} in degree-days and RMSE found for each crop in function of the number of optimization process iteration. The first and third quartile and the median of T_{diff} and RMSE for each crop field are represented. Red crosses stand for outliers.

HESSD
11, 7689–7732, 2014

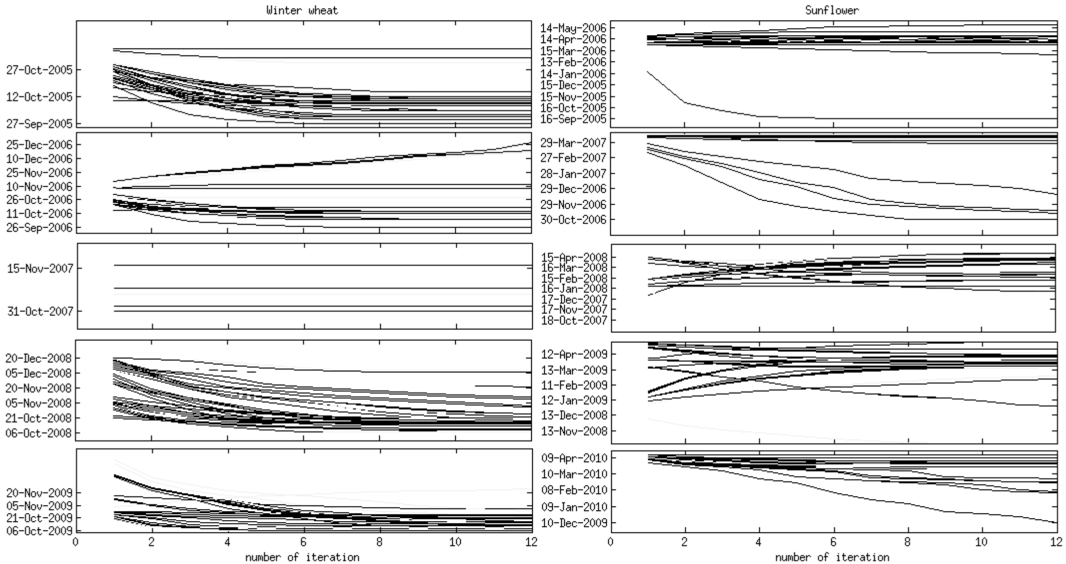

Figure 6. Seeding date trajectories for each crop field as a function of the iteration number.

HESSD
11, 7689–7732, 2014

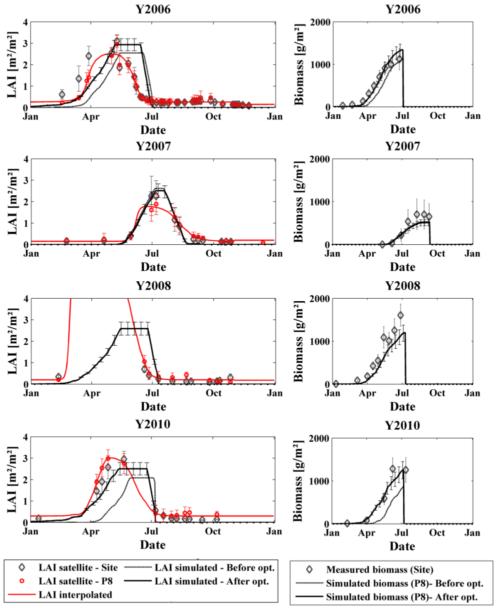

Figure 7. LAI and biomass simulated for 4 years in the crop within the catchment that exhibits cropping pattern comparable to the experimental crop field (except in 2009) where the ground measurement are done. Rows stand for respectively the winter wheat 2006, sunflower 2007, winter wheat 2008 and winter wheat 2010. LAI in the first column: the red curve is the interpolated LAI profile from the F2 derived values (red circles) with the spatial variability represented by the whisker. The black diamonds stand for the F2-LAI values for the experimental crop field located outside the catchment. Black solid and dotted line are the average LAI for respectively after and before seeding date modification; whisker represents the standard deviation of simulated LAI within the crop field. Biomass in the second column is represented in black diamond for the measurements, with the measurement variability associated to the spatial variability and the accuracy of the measurement method. Black solid and dotted line are the average Biomass for respectively after and before seeding date modification; whisker represents the standard deviation of simulated LAI within the crop field.

HESSD
11, 7689–7732, 2014

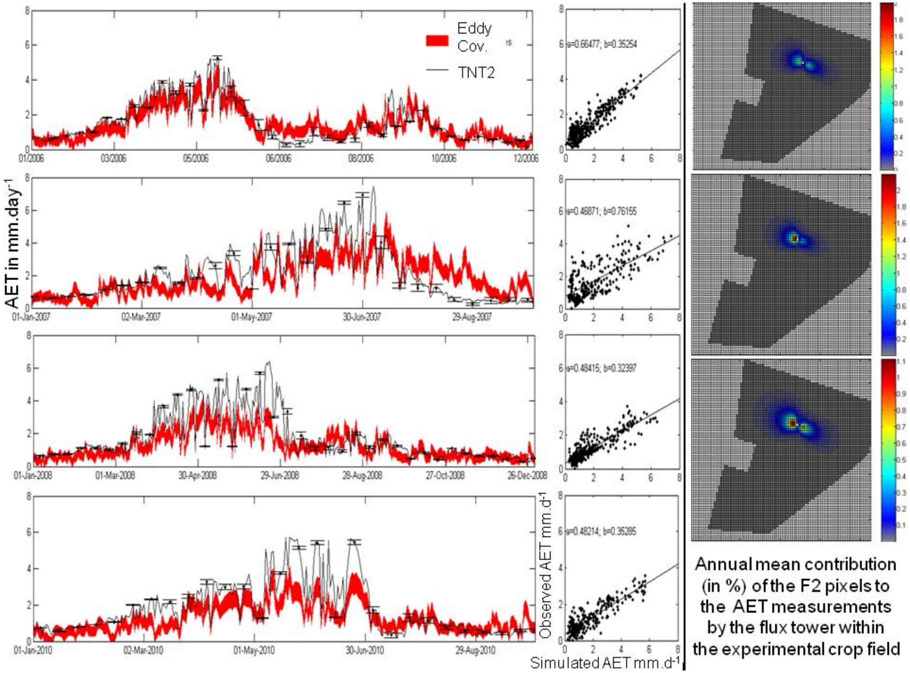

Figure 8. Left panels: measured vs. simulated daily Actual Evapotranspiration respectively from the experimental crop field and the crop field 8. Measured AET are given with the uncertainty envelop associated to the Eddy covariance measurement precision (Béziat et al., 2009). The Nash Sutcliffe coefficient, correlation coefficient (without unit) and RMSE (mm day^{-1}) are respectively 0.57, 0.9 and 0.57 for the year 2006; −0.24, 0.7 and 1.18 for 2007; −0.6, 0.87, 1 for 2008; −0.68, 0.88, 1 for 2010. Linear regression under the form Obs = a × Simulated + b are shown for each year. Right panels: average annual footprint of the flux tower within the experimental crop field computed with the model of Horst (1999). Colors stand for the contribution of each pixel to the AET measured at the tower level (in percentage). Pixel contributions in 2006 are more homogeneously distributed within the footprint than 2007 and 2008 (from unpublished study of E. Potier).

HESSD
11, 7689–7732, 2014

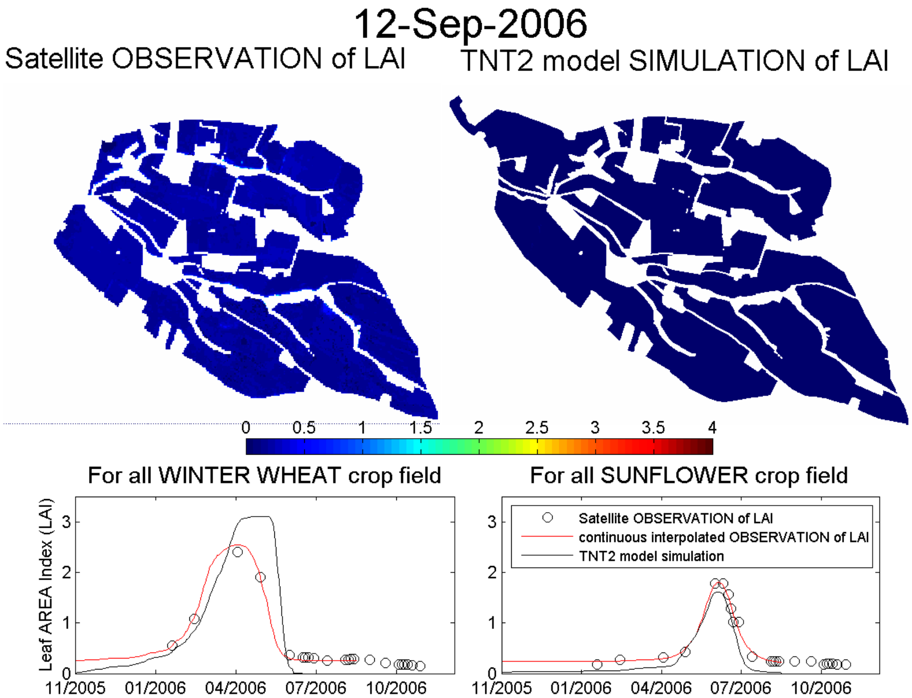

Figure 9. Spatial variability of interpolated LAI derived from F2 series and the TNT2 simulation of LAI. Pixels for which interpolation performances are low are not shown (RMSE > 0.2). The winter wheat LAI is already developed in March, during the sunflower sowing. The opposite situation is represented in July, with the high value of LAI for the sunflower during the wheat senescence. The flow path network and the soil delineation are the main determinants of LAI spatial pattern simulated with TNT2.

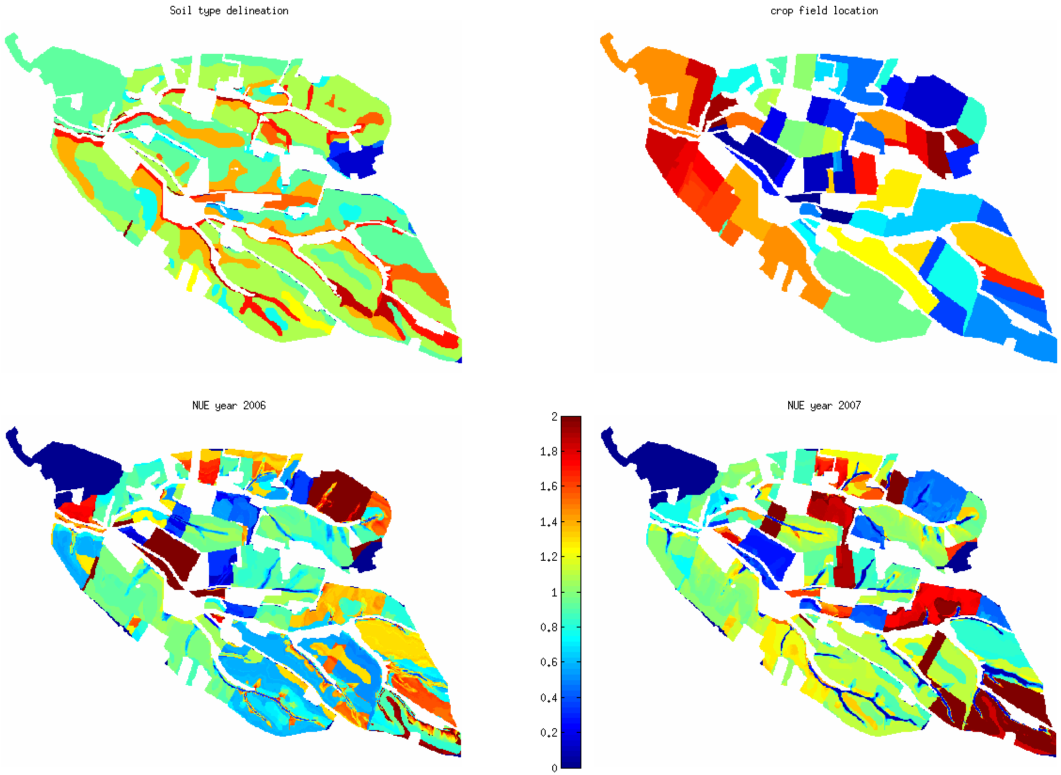

Figure 10. Soil and crop field map used in TNT2 (top). Spatial NUE for the year 2006 and 2007 (respectively bottom left and right panels). The higher the value is, the better the fertilizer is used by the plant. Weak fertilizer amount with weak biomass production could lead to high NUE. Soil organic matter mineralization is a source of mineral nitrogen that lead to NUE higher than one.

HESSD
11, 7689–7732, 2014

Agro-hydrology and multi temporal high resolution remote sensing

S. Ferrant et al.